Inorganic Chemistry

Article

pubs.acs.org/IC

1D Magnetic Interactions in Cu^{II} Oxovanadium Phosphates (VPO), Magnetic Susceptibility, DFT, and Single-Crystal EPR

Diego Venegas-Yazigi,*[,†,‡] Evgenia Spodine,*[,§,‡] Marianela Saldias,[§,‡] Andrés Vega,[⊥,‡] Verónica Paredes-García,[⊥,‡] Rafael Calvo,[¶] and Ricardo Costa de Santana*[,∥]

[†]Facultad de Química y Biología, Universidad de Santiago de Chile, USACH, Santiago, Chile

[‡]Centro para el Desarrollo de Nanociencias y Nanotecnología, CEDENNA, Santiago, Chile

[§]Facultad de Ciencias Químicas y Farmacéuticas, Universidad de Chile, Santiago, Chile

[⊥]Departamento de Ciencias Químicas, Universidad Andrés Bello, Santiago, Chile

[¶]Departamento de Física, Facultad de Bioquímica y Ciencias Biológicas, and Instituto de Física del Litoral, CONICET-Universidad Nacional del Litoral, 3000 Santa Fe, Argentina

[∥]Instituto de Física, Universidade Federal de Goiás, CP 131, 74001-970 Goiânia, Brazil

Supporting Information

ABSTRACT: We report the crystal face indexing and molecular spatial orientation, magnetic properties, electron paramagnetic resonance (EPR) spectra, and density functional theory (DFT) calculations of two previously reported oxovanadium phosphates functionalized with Cu^{II} complexes, namely, $[Cu(bipy)(VO_2)(PO_4)]_n$ (**1**) and $[\{Cu(phen)\}_2(VO_2(H_2O)_2)(H_2PO4)_2\ (PO_4)]_n$ (**2**), where bipy = 2,2′-bipyridine and phen = 1,10-phenanthroline, obtained by a new synthetic route allowing the growth of single crystals appropriate for the EPR measurements. Compounds **1** and **2** crystallize in the triclinic group $P\bar{1}$ and in the orthorhombic *Pccn* group, respectively, containing dinuclear copper units connected by two −O−P−O− bridges in **1** and by a single −O−P−O− bridge in **2**, further connected through −O−P−O−V−O− bridges. We emphasize in our work the structural aspects related to the chemical paths that determine the magnetic properties. Magnetic susceptibility data indicate bulk antiferromagnetism for both compounds, allowing to calculate $J = -43.0\ cm^{-1}$ ($d_{Cu-Cu} = 5.07$ Å; J defined as $H_{ex}(i,j) = -J\ \mathbf{S}_i \cdot \mathbf{S}_j$), considering dinuclear units for **1**, and $J = -1.44\ cm^{-1}$ ($d_{Cu-Cu} = 3.47$ Å) using the molecular field approximation for **2**. The single-crystal EPR study allows evaluation of the **g** matrices, which provide a better understanding of the electronic structure. The absence of structure of the EPR spectra arising from the dinuclear character of the compounds allows estimation of weak additional exchange couplings $|J'| > 0.3\ cm^{-1}$ for **1** ($d_{Cu-Cu} = 5.54$ Å) and a smaller value of $|J'| \geq 0.15\ cm^{-1}$ for **2** ($d_{Cu-Cu} = 6.59$ Å). DFT calculations allow evaluating two different exchange couplings for each compound, specifically, $J = -36.60\ cm^{-1}$ ($d_{Cu-Cu} = 5.07$ Å) and $J' = 0.20\ cm^{-1}$ ($d_{Cu-Cu} = 5.54$ Å) for **1** and $J = -1.10\ cm^{-1}$ ($d_{Cu-Cu} = 3.47$ Å) and $J' = 0.01\ cm^{-1}$ ($d_{Cu-Cu} = 6.59$ Å) for **2**, this last value being in the range of the uncertainties of the calculations. Thus, these values are in good agreement with those provided by magnetic and single-crystal EPR measurements.

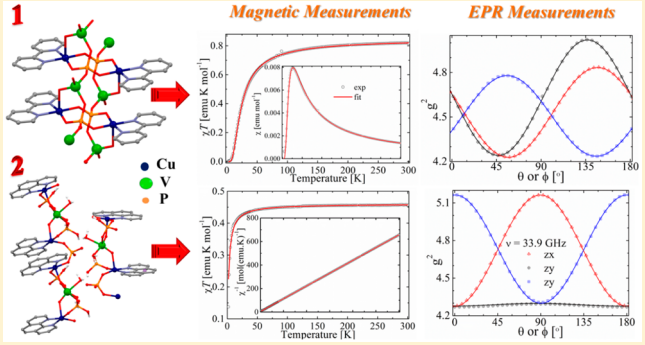

INTRODUCTION

Materials science focuses attention on the design and synthesis of hybrid materials derived from oxometallic inorganic lattices due to the possibility of varying their physicochemical properties functionalizing with both coordination compounds and/or organic molecules. Diamagnetic $V^{V}PO$ lattices can be functionalized with paramagnetic coordination compounds such as Cu^{II} complexes, which also modify the dimensionality of the matrix.[1−6] They offer possibilities to host the complexes, and to provide pathways for superexchange couplings conferring cooperative magnetic properties to the material. Research in the field of hybrid compounds based on phosphovanadium oxides concentrates on the following materials: (a) oxovanadium phosphate or phosphonate with charge-compensating organic cations;[7−10] (b) oxovanadium phosphates with directly coordinated organic ligands,[11−17] (c) oxovanadium phosphates with transition metal ion complexes.[18−20] The obtained compounds allow studying the role of −O−P−O− and −O−V−O− bridges, and their combinations, in supporting exchange interactions between Cu^{II} centers.[21−23]

A new synthetic route and structural, magnetic, and electron paramagnetic resonance (EPR) studies of two VPO lattices

Received: December 19, 2014
Published: April 1, 2015

DOI: 10.1021/ic503045d
Inorg. Chem. 2015, 54, 3805−3814

functionalized with Cu^{II} complexes $[Cu(bipy)(VO_2)(PO_4)]_n$ (**1**) (reported previously by Shi et al.[24]) and $[\{Cu(phen)\}_2(VO_2(H_2O)_2)(H_2PO4)_2\ (PO_4)]_n$ (**2**) (reported previously by Cui et al.[25]) are presented. Magnetic susceptibility data describe the bulk magnetic behavior. Single-crystal EPR spectroscopy applied for the first time to study VPO chains allows detection of small exchange couplings in the presence of larger couplings, and also the principal axes of the g-tensors of the copper centers, that are correlated with the molecular structure, thus allowing a better understanding of underlying phenomena in these materials. Density functional theory (DFT) calculations complete this characterization with a theoretical analysis of the interactions.

EXPERIMENTAL SECTION

Synthesis and Characterization. All chemicals were of reagent grade and used without further purification. Reactions were performed in 23 mL Teflon-lined stainless steel containers. After the reactions finished, the reactors were removed from the oven and allowed to cool to room temperature. Initially we used the methods reported by Shi et al.[24] to prepare compound **1** and those of Cui et al.[25] to prepare compound **2**; these failed to give suitable single crystals for EPR measurements. Thus, we used modified synthetic methods described below, obtaining larger single crystals of good quality as needed for single-crystal EPR measurements.

*$[Cu(bipy)(VO_2)(PO_4)]_n$ (**1**).* CuO (0.1935 g, 2.43 mmol), 2,2-bipyridine (0.0734 g, 0.47 mmol), H_3PO_4 (0.41 g, 4.2 mmol), $NaVO_3$ (0.0875 g, 0.72 mmol), and H_2O (10 mL, 555.56 mmol) in 5.2:1:8.9:1.5:1182 molar ratio were mixed in the reactor and heated under autogenous pressure at 200 °C for 4 d. The initial pH value of the reaction mixture was 1.3. After the reaction solution had cooled to room temperature, the products were filtered off and dried at 40 °C. Rectangular blue crystals corresponding to $[Cu(bipy)(VO_2)(PO_4)]_n$ displaying (010) growth faces and edges along [100] direction were obtained and separated manually (yield: 30.4% based on V). In the present work more acidic conditions were used than those reported by Shi et al.,[24] leading to crystals of adequate size for single-crystal EPR measurements.

*$[\{Cu(phen)\}_2(VO_2(H_2O)_2)(H_2PO4)_2(PO_4)]_n$ (**2**).* $CuCl_2{\cdot}2H_2O$ (0.2866 g, 1.68 mmol), 1,10-phenanthroline (0.1533 g, 0.85 mmol), NaH_2PO_4 (1.200 g, 10 mmol), $NaVO_3$ (0.1033 g,0.85 mmol), Zn (0.1055 g, 1.61 mmol), and H_2O (5 mL, 277 mmol) in 1.9:1:11.8:1:1.9:326 molar ratio were mixed in the reactor and heated under autogenous pressure at 120 °C for 3 d. The initial pH value of the reaction mixture was 2.8. Blue rod-shaped crystals of $[\{Cu(phen)\}_2(VO_2(H_2O)_2)(H_2PO4)_2(PO_4)]_n$ displaying largest (001) growth faces with edges along the [100] direction were obtained together with other byproducts, which were filtered off and dried at 40 °C; the crystals were separated manually (yield: 9.6% based on V). Even though the synthetic conditions used in the present work produced a lower yield than that reported by Cui et al.,[25] the differences in the nature of the reagents and the used temperature permitted to obtain larger crystals, which were adequate for single-crystal EPR measurements. Besides, the presence of metallic zinc in the hydrothermal reaction to induce crystallization was introduced, whose utility in the crystallization process has been proven before.[19,26] It is important to stress that several experiments were performed to improve the quality of the crystals, but no general method was found. For example, the use of metallic zinc proved to be useful for **2** but not in the case of **1**.

Experimental Techniques. Infrared spectra of pressed KBr pellets were recorded on a PerkinElmer FT-IR spectrometer Spectrum Two, in the 4000−400 cm^{-1} region. Elemental analyses (C,H,N) were performed on a CE Instruments, ED 1108 Elemental Analyzer.

*Results for **1**.* IR, cm^{-1}: 1101(s), 1055 (s) bands are assigned to the P−O stretching mode, band at 955 (m) is due to stretching vibrations of the terminal V═O group, while 885 (s), 852 (w) are assigned to V−O−V stretching vibrations. 721 (s); 503 (w), 494 (w) correspond to stretching vibrations of V−O or V−O−P bonds; 1628 (m), 1608 (m), 1425 (s) correspond to the 2,2-bipyridine ligand. Anal. Calcd for $C_{10}H_8CuN_2O_6PV$: C, 30.17; H, 2.01; N, 7.04%. Found: C, 29.7; H, 2.5; N, 6.0%.

*Results for **2**.* IR, cm^{-1}: 1045(s), 1007 (m) bands are assigned to P−O stretching, 964 (s), 943 (m) are assigned to V−O−V stretching vibrations; 721 (w), 503 (w) correspond to stretching vibrations of V−O or V−O−P bonds; 1632 (m), 1520 (m), 1429 (s) correspond to the organic ligand 1,10-phenanthroline. Anal. Calcd for $C_{24}H_{24}Cu_2N_4O_{16}P_3V$: C, 32.47; H, 1.81; N, 6.31%. Found: C, 31.5; H, 2.2; N, 6.1%.

X-ray Diffraction Methods. The data were collected on a Bruker Smart Apex diffractometer at 293 K, using separations of 0.3° between frames, and 10 s by frame. Data integration was made using SAINTPLUS.[27] The structures of **1** and **2** were solved by direct methods using XS in SHELXTL[28] and completed (non-H atoms) by Fourier difference synthesis. Refinement until convergence was obtained using XL SHELXTL and SHELXL97.[29] All hydrogen atoms were calculated in idealized positions on geometric basis and refined with restrictions. Table 1 summarizes the methods used and displays the main structural parameters obtained for compounds **1** and **2**.

Table 1. Crystallographic Parameters for 1 and 2

	1	2
empiric formula	$CuC_{10}H_8O_6N_2PV$	$Cu_2C_{24}H_{24}O_{16}N_4P_3V$
formula weight	397.64	895.42
temperature (K)	296(2)	298(2)
wavelength (Å)	0.71073	0.71073
crystal system	triclinic	orthorhombic
space group	$P\bar{1}$ (No. 2)	*Pccn* (No. 56)
a (Å)	5.5358(2)	10.0539(10)
b (Å)	10.254(3)	12.762 (12)
c (Å)	11.750(4)	22.749(2)
α (deg)	74.43(10)	90.00
β (deg)	79.87(10)	90.00
γ (deg)	85.71(2)	90.00
volume ($Å^3$)	635.27(4)	2919.0(5)
Z	2	4
density (calcd)	2.089	2.037
coeff absorption	2.576	2.012
F(000)	394	1800
goodness-of-fit on F^2	1.096	1.035
final *R* indices ($I > 2\sigma(I)$)	*R*1 = 0.0187	*R*1 = 0.0261
	*wR*2 = 0.0567	*wR*2 = 0.0782
indices (all data)	*R*1 = 0.0192	*R*1 = 0.0276
	*wR*2 = 0.0565	*wR*2 = 0.0772

Magnetic Measurements. The magnetic susceptibilities of powder samples of **1** (47.0 mg) and **2** (39.2 mg) were measured in the temperature range of 2−300 K with a field of 100 mT, using a Quantum Design SQUID magnetometer MPMS-XL5. All experimental data were corrected for diamagnetism estimated from Pascal constants and temperature-independent paramagnetism (TIP) (-1.2×10^{-4} emu mol^{-1} for **1** and -2.8×10^{-4} emu mol^{-1} for **2**).[30] The used molecular weights to obtain the molar susceptibility were 795.28 for **1** and 447.71 for **2**.

Electron Paramagnetic Resonance Techniques. Spectra of single-crystal and powder samples of both compounds were collected at ∼33.9 and ∼9.7 GHz (Q and X-bands, respectively) and room temperature using a Bruker ESP-300 spectrometer, with standard Bruker cavities operating with ∼0.8 mT of 100 kHz magnetic field modulation and a microwave power of ∼20 mW. The magnetic field $\mathbf{B}_0 = \mu_0\mathbf{H}$ (μ_0 is the permeability of the vacuum) at the position of the sample was calibrated using a speck of diphenylpicrylhydrazyl (dpph, g = 2.0036) as field marker. Powder samples were made by grinding selected single crystals. For the single-crystal EPR studies the

DOI: 10.1021/ic503045d
Inorg. Chem. 2015, 54, 3805−3814

orientations of $\mathbf{B}_0$ in the crystal axes were attained by gluing the largest growth face of a single crystal to cubic KBr single-crystal sample holders obtained by cleavage, with a natural crystal edge along one side of the cube, which defines an *xyz* set of orthogonal axes. Knowledge of the growth habit of the crystals allows relating this "laboratory" *xyz* system to the crystallographic axes. For the triclinic compound **1**, $x = a$, the [100] direction, $y \equiv b^* = c \times a/|c \times a|$ (normal to the (010) growth face), and $z \equiv c^* = a \times b^*/|a \times b^*|$. The crystallographic data in the triclinic system were transformed[31,32] to the set of orthogonal axes $xyz \equiv ab^*c^*$ to correlate the EPR results to the crystal structure. For the orthorhombic compound **2**, $x \| a$, $y \| b$, and $z \| c$, and no transformation is needed. The holders were positioned on a pedestal inside the microwave cavity, and the orientation of the external magnetic field $\mathbf{B}_0$ in the coordinate system of the holder was varied by rotating the magnet. The spectra were recorded at 5° orientation intervals for the external magnetic field in a range from 0° to 180° in the three *xy*, *yz*, and *zx* orthogonal planes. Positions and peak-to-peak line widths (ΔB_0) of the resonance lines were obtained by least-squares fittings of a Lorentzian derivative line shape to the observed spectra. The positions of the crystal axes in the three orthogonal planes can be accurately defined when there is an axis of symmetry in these planes, which should be reflected by the angular variations of the *g*-factor and the line width. This task is less accurate in triclinic crystals lacking an axis of symmetry. The values of $g^2(\theta,\phi)$ and $\Delta B_0(\theta,\phi)$ for any crystal direction at Q- and X-bands are very similar, the better quality results being mostly at Q-band, described and discussed in this work. The results at X-band do not add much information, and we add a comment about this point. The EPR data were analyzed with EasySpin,[33] a program package working under Matlab.[34]

Density Functional Theory Calculations. Spin-unrestricted calculations under the DFT were done using the hybrid B3LYP functional[35] and a triple-ζ all-electron basis set for all atoms.[36] A guess function, generated using Jaguar 5.5 code,[37] and using a triple-ζ basis set, was used for all atoms. Total-energy calculations were performed with the Gaussian09 program,[38] using the quadratic convergence method with a convergence criterion of 1×10^{-7} a.u. Mulliken spin densities were obtained from the Gaussian09 single-point calculations. Using the nonprojected energy of the broken-symmetry solution as the energy of the low spin state within the DFT methodology gives good results because it avoids the cancellation of the nondynamic correlation effects, as stated in studies performed by Ruiz et al.[39] Thus, the *J* value is obtained using the nonprojected method proposed by the same authors:[40]

$$E_{HS} - E_{BS} = -J(2S_1S_2 + S_2) \quad (1)$$

where S_1 and S_2 are the total spins of the two interacting paramagnetic centers with $S_1 \geq S_2$, using the Heisenberg Hamiltonian for **1** (eq 2a) and **2** (eq 2b):

$$H_{HDVV} = -J(S_1 \cdot S_2 + S_3 \cdot S_4) - J'(S_1 \cdot S_3 + S_2 \cdot S_4) - J''(S_1 \cdot S_4) - J'''(S_2 \cdot S_3) \quad (2a)$$

For **1**, $J''' = 0$, due to the Cu2−Cu3 distance of 8.167 Å.

$$H_{HDVV} = -J(S_1 \cdot S_2 + S_3 \cdot S_4) - J'(S_2 \cdot S_3) \quad (2b)$$

RESULTS AND ANALYSIS

Structural Description. Selected distances and angles of structures **1** and **2** are given in Tables 2 and 3, respectively. The bond valence sum (BVS) for the vanadium atom is 5.02 for **1** considering tetrahedral geometry and 4.98 for **2** considering octahedral sites. For the copper atom it is 1.90 for **1** and 2.03 for **2**, considering in both cases square pyramidal geometry.[41] These values fit well with the oxidation states V^V and Cu^{II} deduced from the observed crystal structures.

[Cu(bipy)(VO$_2$)(PO$_4$)]$_n$ (1). Triclinic compound **1** consists of $\{Cu(bipy)\}^{2+}$ cationic units linked to a $\{(VO_2)(PO_4)\}_n$ skeleton in a one-dimensional (1D) array parallel to the [100] direction with V^V and P^V atoms in tetrahedral environments. The Cu^{II} ions display a square pyramidal coordination geometry (τ = 0.10),[42] defined by two nitrogen atoms (N1 and N2) belonging to the 2,2′-bipyridine ligand, two oxygen atoms (O1 and O3) from two different phosphate groups, while the apical position is occupied by one oxygen atom (O5) from a tetrahedral vanadate group (Table 2). Each Cu^{II} atom links three oxygen atoms from adjacent VO_4 and PO_4 tetrahedra from one chain, and a PO_4 group from the

Table 2. Selected Distances and Angles for [Cu(bipy)(VO$_2$)(PO$_4$)]$_n$ (1)

distances (Å)	angles (deg)
Cu−O3 1.9207(12)	O3−Cu1−O1 93.94(5)
Cu−O1 1.9180(13)	O3−Cu1−N1 167.69(6)
Cu−N1 1.9925(15)	O1−Cu1−N2 173.33(6)
Cu−N2 1.9969(16)	N1−Cu1−N2 80.98(7)
Cu−O5 2.3510(14)	O1−Cu1−O7 90.18(6)
Cu1···Cu1^{i} 5.067(2)	O3−Cu1−N2 92.07(6)
Cu1···Cu1 5.536(2)	N1−Cu1−O5 100.13(6)
	N2−Cu1−O5 91.13(5)
V1−O4 1.8548(13)	
V1−O5 1.6265(13)	O4−V1−O5 109.91(6)
V1−O2 1.8407(13)	O5−V1−O2 111.61(7)
V1−O6 1.6124(14)	O4−V1−O6 106.83(7)
	O5−V1−O6 107.98(7)
P1−O3 1.5103(13)	O2−V1−O6 107.10(7)
P1−O1 1.5046(14)	
P1−O2 1.5575(13)	O1−P1−O4 109.61(8
P1−O4 1.5636(13)	O1−P1−O2 108.04(7)
	O3−P1−O2 109.11(7)
	O3−P1−O1 114.37(8)
	O3−P1−O4 110.83(7)

Table 3. Selected Distances and Angles for [{Cu(phen)}$_2$(VO$_2$(H$_2$O)$_2$)(H$_2$PO$_4$)(PO$_4$)]$_n$ (2)

distances[a] (Å)	angles (deg)
Cu−O5 1.9376(15)	O5−Cu1−N1 90.28(7)
	O6−Cu1−N1 166.87(7)
Cu−O6 1.9245(16)	O1−Cu1−N1 96.33(7)
Cu−N1 2.0110(2)	O1−Cu1−O6 95.69(6)
Cu−N2 2.0172(18)	N1−Cu1−N2 81.35(7)
Cu−O1 2.2436(15)	O1−Cu1−O5 91.17(6)
	O6−Cu1−O5 94.74(7)
Cu···Cu1^{i} 6,591(2)	O5−Cu1−N2 170.03(7)
Cu1^{i}···Cu1^{ii} 3.465(2)	
V1−O1 1.6371(15)	O1−V1−O2 101.16(7)
V1−O1W 2.2897(17)	O1W−V1−O1 167.81(7)
V1−O2 1.9605(15)	O2−V1−O1W 78.17(6)
P1−O5 1.5102(15)	O3−P1−O1 110.04(10)
P1−O2 1.5166(16)	O3−P1−O2 110.30(9)
P1−O3 1.5424(15)	O2−P1−O4 108.69(9)
P1−O4 1.5696(16)	O3−P1−O4 103.79(9)
	O5−P1−O2 114.25(9)
P2−O6 1.5332(16)	O1−P1−O4 107.89(10)
P2−O7 1.5408(15)	O6−P2−O6 108.94(19)
P2−O6^{i} 1.5336(2)	O6−P2−O7 109.16(8)
P2−O7^{i} 1.5408(15)	O6−P2−O7 107.41(8)
	O7−P2−O7 113.15(14)
	O10−P2−O8 108.96(15)
	P1−O4−H4P 118.92(13)

[a]Symmetry codes: (i) $-1/2 - x, -1/2 - y, z$; (ii) $-1 + x, y, z$.

DOI: 10.1021/ic503045d
Inorg. Chem. 2015, 54, 3805−3814

neighboring chain, to form a double $\{(VO_2)(PO_4)\}_n$ 1D structure (Figure 1). As a result of the formed double-stranded

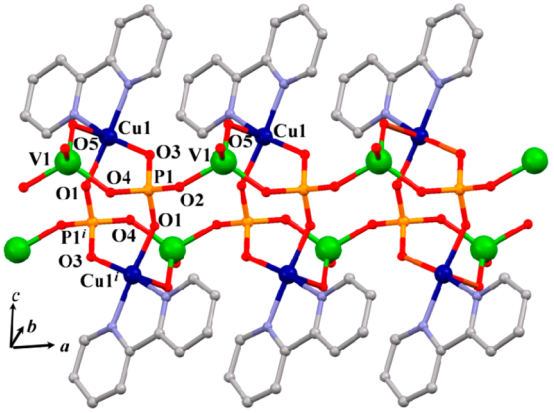

Figure 1. View of the chain structure for $[Cu(bipy)(VO_2)(PO_4)]_n$ **1** running along the *a* axis. Symmetry code (i) $2 - x, 1 - y, -z$.

chains there are two crystallographically equivalent Cu^{II} atoms within a dinuclear unit (Cu1···Cu1^i at 5.067 (3)Å; (i) $2 - x, 1 - y, -z$) related by an inversion center and bonded through two equatorial−equatorial phosphate bridges Cu_{eq}−O1−P1−O3−Cu_{eq}, with a bond distance of 6.853 Å and a bridge angle O1−P1−O3 of 114.37(8)°. These dinuclear units can be considered as the rungs of the ladder defined by the double-stranded chain. Another dinuclear unit bonded with a distance of 5.536(3) Å between Cu1···Cu1 atoms and bridged by an equatorial−axial phosphovanadate bridge (Cu_{ax}−O5—V1−O2−P1−O3−Cu_{eq}, 10.806 Å) is observed along the *c* axis. In the 1D structure the rings from adjacent 2,2′-bipyridine ligands provide weak $\pi-\pi$ intrachain interactions, ca. 3.5 Å with a slippage angle of 16.1° (Supporting Information, Figure S1). Hydrogen atoms of the 2,2′-bipyridine ligand form nonbonded contacts with two O atoms from one oxovanadium group of the neighboring chain. This weak interaction occurs between atoms C9···O5^i (3.331(3) Å) and C8···O6^i (3.335(3) Å), (i) $x, y, z + 1$.

[{Cu(phen)}$_2$(VO$_2$(H$_2$O)$_2$)(H$_2$PO$_4$)$_2$ (PO$_4$)]$_n$ (**2**). Orthorhombic compound **2** displays a 1D structure described by $\{Cu(phen)\}^{2+}$ units linked by PO_4 groups, forming dinuclear units. These units are further connected by $\{VO_2(H_2O)_2(H_2PO_4)_2\}$ bridges, giving rise to chains parallel to the [100] direction (Figure 2) with the vanadium atom in (VO_6) octahedral environment. The expanded chain allows defining two

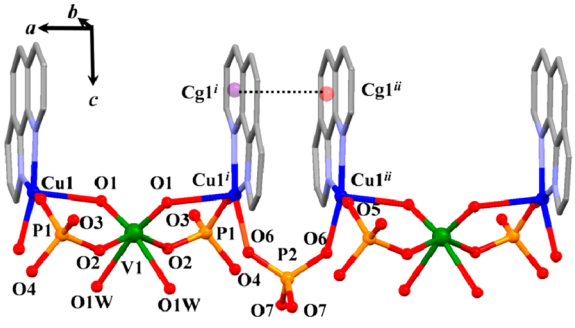

Figure 2. View of structure for $[\{Cu(phen)\}_2(VO_2(H_2O)_2)(H_2PO_4)(PO_4)]_n$ **2** running along the *a* axis. Symmetry codes (i) $-1/2 - x, 1/2 - y, z$, (ii) $-1 + x, y, z$. Cg1: N1 C8 C9 C11 C12 C10.

dinuclear Cu···Cu distances with different bridges. The intradinuclear distance between $\{Cu(phen)\}^{2+}$ entities is 3.465(3) Å (Cu1^i···Cu1^{ii}; (i) $-1/2 - x, 1/2 - y, z$, (ii) $-1 + x, y, z$) and the equatorial−equatorial chemical paths are provided by a PO_4 bridge (Cu1^i−O6−P2−O6−Cu1^{ii}, with a total σ bond distance of 6.922 Å). The apical−apical bridges between Cu1···Cu1^i at 6.591(3) Å, Cu1−O1−V1−O1−Cu1^i have a total distance of 7.762 Å and contain three diamagnetic atoms. 1,10-Phenanthroline ligands are located on one side of the 1D structure, and the rings belonging to adjacent 1,10-phenanthroline ligands are at ca. 3.5 Å generating $\pi-\pi$ stacking interactions, with a slippage angle of 20.0° (Supporting Information, Figure S2). Hydrogen atoms of the H_2PO_4 groups and oxygen atoms of $VO_2(H_2O)_2$ groups from the neighboring chain are forming hydrogen bonds. This interaction allows the structural stabilization of the chains along the axis of growth. The hydrogen bonds are O1W···O4^{ii} (2.896(3) Å; (ii) $-x, y - 1/2, 1/2 - z$).

Magnetic Properties. Figure 3a,b displays the *T* dependence of the χT (a) and $\chi(T)$ (b) corresponding to 1 mol of

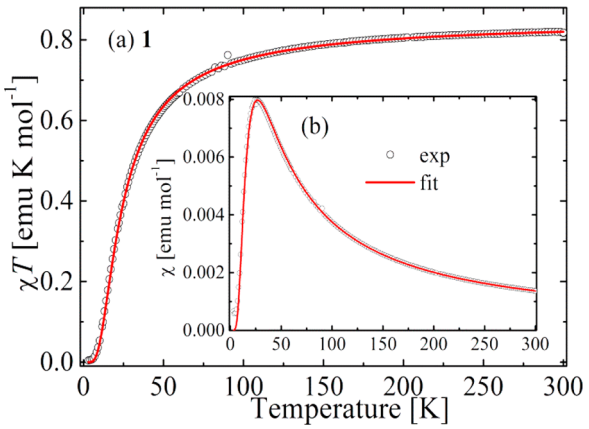

Figure 3. Temperature dependence of χT (a) and $\chi(T)$ (b) for **1**. Circles (○) represent the experimental results, and the red lines correspond to the fit with the Bleaney−Bowers equation as described in the text.

dinuclear units per formula of **1**. At 300 K, χT = 0.80 emu·mol^{-1} K indicating a *g* value of 2.09 and effective magnetic moment per Cu of 1.80 μ_B. The χT curve (a) decreases sharply at low temperatures, indicating dominant antiferromagnetic (AF) interactions; $\chi(T)$ (b) displays a maximum value at 27.2 K, as is usually obtained for dinuclear compounds.[43]

Figure 4a,b displays $\chi T(T)$ (a) and the inverse susceptibility $\chi^{-1}(T)$ (b) for one mol of Cu of **2**. At room temperature χT = 0.46 emu·mol^{-1} K, consistent with one Cu^{II} center per formula having g = 2.12 and an effective magnetic moment of 1.92 μ_B. As observed for **1** the χT curve indicates predominant AF interactions for **2**. No maximum in the studied temperature range is observed in the $\chi(T)$ curve for compound **2** (not shown) above 2 K.

Powder Electron Paramagnetic Resonance Spectra of 1 and 2. Figure 5a,b displays powder EPR spectra ($d\chi''/dB_0$) at Q-band for **1** and **2**, respectively, observed at room temperature. They are typical of $S = 1/2$ Cu^{II} ions in square planar or square pyramidal coordinations, with no fine (dinuclear) or hyperfine splitting. The principal values of the anisotropic *g*-matrices $g_1 = g_2 = g_\perp = 2.057(3)$, $g_3 = g_\parallel = 2.262(3)$ for **1** and $g_1 = 2.071(2)$, $g_2 = 2.072(3)$, and $g_3 =$

DOI: 10.1021/ic503045d
Inorg. Chem. 2015, 54, 3805−3814

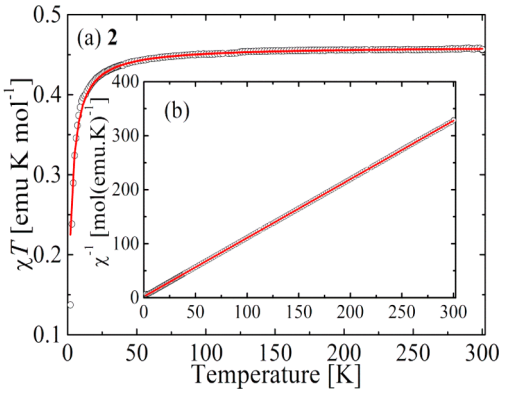

Figure 4. Temperature dependence of χT (a), and $\chi^{-1}(T)$ for **2**. Circles (○) represent the experimental results, and the red lines correspond to the fit with Curie−Weiss equation as described in the text.

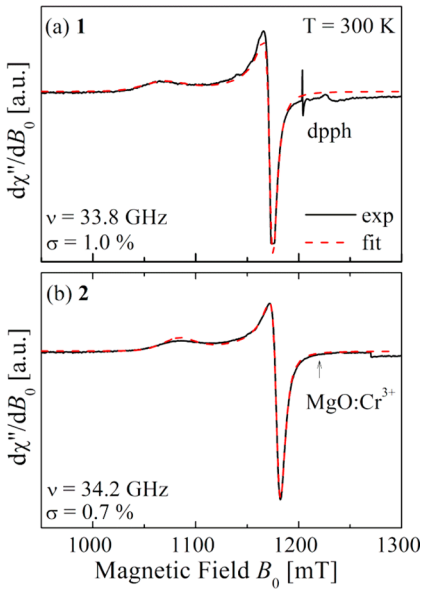

Figure 5. EPR spectrum of powder samples of (a) **1** and (b) **2**, obtained at Q-band and room temperature. Solid and dashed lines are, respectively, the experimental results and the simulation obtained using the parameters given in the text. σ is the rms deviation of the simulation from the data (see text).

2.258(3) for **2** were calculated from these spectra using EasySpin.[33] The spectra calculated with these parameters, shown as dashed lines in Figure 5a,b, are in good agreement with the experimental results, displaying root-mean-square (rms) deviations $\sigma = [(1/N_p)\sum_i(S_{exp,i} - S_{sim,i})^2]^{1/2} = 1.2\%$ and 0.7% for **1** and **2**, respectively, where S indicates the experimental and simulated signal amplitudes, and the sum runs over the N_p points j of the spectra.

Single-Crystal Electron Paramagnetic Resonance Spectra. A single resonance line without hyperfine splitting was observed for all orientations of $\mathbf{B_0}$ in the three orthogonal planes of compounds **1** and **2**. Their squared g factors in the three studied planes (Figure 6a,b) were calculated from positions obtained, proposing Lorentzian line shapes, as expected for exchange-narrowed resonances and observed in the data.

The spectra observed for a dinuclear unit with copper atoms A and B coupled by an isotropic AF exchange and by

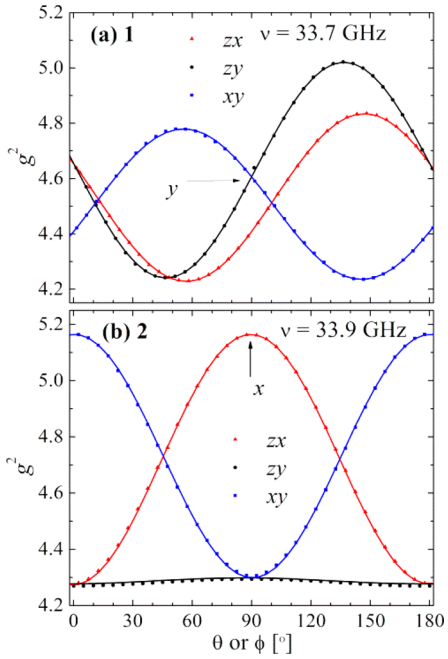

Figure 6. Experimental values of the g^2 factor at Q-band and room temperature for $\mathbf{B_0}$ applied in the three orthogonal laboratory planes xy, zx, and zy of compounds **1** (a) and **2** (b). Symbols are the experimental values. The solid lines were obtained with the components of g^2 given in Table 4, obtained from global fits of eq 4 to the data in the three planes.

anisotropic interactions (sum of anisotropic exchange plus dipole−dipole couplings) should obey the spin Hamiltonian:[44]

$$\mathcal{H}_S = \mu_B(\mathbf{S_A}\cdot\mathbf{g_A}\cdot\mathbf{B_0} + \mathbf{S_B}\cdot\mathbf{g_A}\cdot\mathbf{B_0}) - J\mathbf{S_A}\cdot\mathbf{S_B} + \mathbf{S_A}\cdot\mathbf{D}\cdot\mathbf{S_B} \quad (3)$$

where μ_B is the Bohr magneton, S_A and S_B are effective spin 1/2 operators, and g_A and g_B are the molecular **g**-matrices, equal for copper sites related by an inversion operation in **1**, and related by a C_2 operation in **2**.

The AF exchange coupling term $-J\mathbf{S_A}\cdot\mathbf{S_B}$ splits the levels in a ground singlet and an excited triplet with energy J, where two allowed EPR transitions, $\Delta M_S = \pm 1 \leftrightarrow 0$, occur. The **D** term of eq 3 considers anisotropic exchange and dipolar interactions giving rise to an angular dependent splitting of these lines that should be observed if $|\mathbf{D}|/g\mu_B$ is larger than the EPR line width. The two principal values of the traceless **D** matrix, D and E, could be determined from the angular variation of this splitting in single crystal samples. Since the observed spectra do not show such dinuclear splitting, either $|\mathbf{D}|$ is negligible, or the coupling $|J'|$ between neighboring dinuclear units is larger than $|\mathbf{D}|$, and a single collapsed resonance is observed for the two copper spins (see later).[45−49] The observed single-line EPR results was interpreted proposing a crystal **g** matrix, average of the molecular $\mathbf{g}_i$ matrices of the two copper sites, equal for **1**, and related by a C_2 rotation in **2**. Least squares fitting of the function:

$$\begin{aligned} g^2(\theta,\phi) = {} & (g^2)_{xx}\sin^2\theta\cos^2\phi + (g^2)_{yy}\sin^2\theta\sin^2\phi \\ & + (g^2)_{zz}\cos^2\theta + 2(g^2)_{xy}\sin^2\theta\sin\phi\cos\phi \\ & + 2(g^2)_{xz}\sin\theta\cos\theta\cos\phi \\ & + 2(g^2)_{yz}\sin\theta\cos\theta\sin\phi \end{aligned} \quad (4)$$

DOI: 10.1021/ic503045d
Inorg. Chem. 2015, 54, 3805−3814

Table 4. Components of the Crystal g^2 Matrix for Compounds 1 and 2[a]

	compound 1	compound 2
ν	33.6 GHz	33.9 GHz
$(g^2)_{xx}$	4.4082(5)	5.1654(8)
$(g^2)_{yy}$	4.6066(5)	4.2751(8)
$(g^2)_{zz}$	4.6543(4)	4.296(1)
$(g^2)_{xy}$	0.2536(6)	0.005(1)
$(g^2)_{xz}$	−0.2774(6)	0.007(1)
$(g^2)_{yz}$	−0.3898(6)	0.001(1)
$(g^2)_1$	4.2278(6)	4.2750(8)
$(g^2)_2$	4.2419(7)	4.2961(10)
$(g^2)_3$	5.1994(7)	5.1655(8)
$\boldsymbol{a}_1$	[0.84(3), −0.01(1), 0.54(2)]	[0.008(1), 0.06(5), −0.998(5)]
$\boldsymbol{a}_2$	[0.33(1), −0.786(4), −0.52(2)]	[0.006(1), −0.998(5), −0.06(5)]
$\boldsymbol{a}_3$	[0.429(3), 0.617(3), −0.660(3)]	[0.999 95(1), 0.006(1), 0.008(1)]
crystallographic axial directions	n_{Cu} = [0.514, 0.579, −0.633]	[0.955, ±0.278, ∓0.107] ⟨n⟩ [0.955, 0, 0]
$g_\parallel$	2.2833(4)	2.278(2)
$g_\perp$	2.0561(7)	2.067(2)

[a]Obtained by least-squares fits of the function $g^2(\theta,\phi)$ to the experimental data taken on single crystals at Q-band, displayed in Figure 6. $(g^2)_1$, $(g^2)_2$, $(g^2)_3$ and $\boldsymbol{a}_1$, $\boldsymbol{a}_2$, $\boldsymbol{a}_3$ are the eigenvalues and eigenvectors of the g^2-matrix in the $\boldsymbol{ab^*c^*}$ and in the $\boldsymbol{abc}$ coordinates systems, respectively.

to the experimental values of $g^2(\theta,\phi)$ in Figure 6a,b, provide the elements of the $\boldsymbol{g}^2$ matrices given in Table 4, together with their eigenvalues and eigenvectors. The result of this global fit of eq 4 to the data in the three studied planes, indicated as solid lines in Figure 6a,b, are in good agreement with the data, and provide accuracy matrix elements, eigenvalues and eigenvectors of the $\boldsymbol{g}$-matrices.

The eigenvector a_3 for **1**, shown in Figure 6a and corresponding to $g_\parallel$ (or g_3), lies at (5 ± 1)° with the normal $\boldsymbol{n}_{Cu}$ to the copper equatorial planes defined by the ligands N2, N1, O1, and O3 atoms in the dinuclear unit, reflects copper ions located in approximate axial symmetry.[50] For **2** the g^2 matrix (Table 5) is diagonal in the $xyz \equiv abc$ axes, as required by the orthorhombic crystal symmetry, and nearly axially symmetric with $g_\parallel \approx 2.278$ along the chains (a axis, Figure 7b). According to the structural data for **2**, the vectors n_A and n_B normal to the planes of the ligands to two copper neighbors A and B along one chain, (Cu1 and Cu1^i, Figure 7b), are related by a C_{2a} operation around the axis of the chain, with an angle 2α = 12.9° between them, in good agreement with the EPR result of 2α = 17.5°, obtained using established procedures.[51,52] In both cases the eigenvalues of the **g** matrices reflect the axial symmetry already shown by the EPR spectra of the powder samples, the consequence of a ground state of B_{1g} corresponding to a single electronic occupation of orbital $d(x^2-y^2)$ of the $3d^9$ configuration of the copper ions,[52] as expected for an approximate square pyramidal coordination. All results show that $g_\parallel$ is larger than $g_\perp$, the eigenvector $\boldsymbol{a}_3$ lies in the direction of the $d(z^2)$ orbital, and is normal to the plane of the maximum of the probability amplitude of the $d(x^2-y^2)$ magnetic orbital, in the basal plane (see Figure 7). The differences between widths observed at Q and X bands are less than 10%, indicating that residual Zeeman interactions do not contribute to the EPR broadening.[53]

DISCUSSION

Magnetic Behavior. As shown in Figure 1 and Scheme 1, two bridges connecting the Cu1···Cu1^i nearest neighbors (at 5.07 Å) are observed for $[Cu(bipy)(VO_2)(PO_4)]_n$ (**1**). In the first bridge, the 1,3-PO_4 groups, in a syn−anti coordination mode, are involved in the exchange through three atom equatorial−equatorial −O−P−O− bridges (6.85 Å). The second bridge involves the equatorial−axial paths containing five diamagnetic atoms and condensed vanadium phosphate bridges −O−V−O−P−O− (10.91 Å), and should not be considered as an effective exchange pathway. A bridge −O−P−O−V−O− is responsible for the expansion of the "building block", and thus the generation of the chain. The second exchange pathway is between Cu1 and the next neighboring Cu1 in the chain (Figure 1, Scheme 1).

Since the exchange interaction parameter J decreases with an increasing number of σ bonds in the path, it becomes evident that in the description of the bulk magnetic behavior the phosphate bridge is most important, and the experimental magnetic susceptibility data were successfully analyzed considering dinuclear units with the Hamiltonian of eq 5, using the Bleaney−Bowers equation:[43,54]

$$\chi(T) = \frac{2Ng^2\mu_B{}^2}{k_B T}[3 + \exp(-J/k_B T)]^{-1} \quad (5)$$

where N is Avogadro's number, μ_B is the Bohr magneton, and k_B is the Boltzmann constant. Using g = 2.130 ± 0.005, J = −43.0 ± 0.5 cm^{-1} gives the best fit of the data for χT in the temperature range from 2 to 300 K, with $R = \sum[(\chi_M)_{exp} - (\chi_M)_{calc}]^2/\sum[(\chi_M)_{exp}]^2 = 6.12 \times 10^{-4}$, and the calculated curve is shown in Figure 3a. The negative value of J indicates AF exchange coupling, already shown by the decrease of χ at low T (inset, Figure 3b). This value can be compared to J = −8 cm^{-1} reported for $[Cu_2(phen)_2(H_2O)_2(H_2PO_4)_2](NO_3)_2{\cdot}2H_2O$],[13] where the two metal centers also have a square pyramidal geometry bridged by two syn−anti phosphate groups with Cu···Cu distance of 5.01 Å, comparable to 5.07 Å for compound **1**. In both cases the PO_4 groups form a chairlike arrangement. Considering the definition for the dihedral angle given in ref 13 (defined by the plane of the equatorial ligands to copper and by the plane of the four oxygen atoms of the bridging phosphate groups), 160.8° is calculated for this angle in **1**. Thus, compound **1** is less distorted than $[Cu_2(phen)_2(H_2O)_2(H_2PO_4)_2](NO_3)_2{\cdot}2H_2O]$, (150.8°) and a larger exchange coupling occurs due to a larger overlap between the orbitals responsible for the exchange phenomenon.

DOI: 10.1021/ic503045d
Inorg. Chem. 2015, 54, 3805−3814

Table 5. Comparison of the Magnetic Parameters of 1 and 2 with those for Related Compounds[a]

compound	d_{Cu-Cu}	bridge	coordination form	J^b	ref
(I) $[Cu(bipy)(VO_2)(PO_4)]_n$ (**1**)	5.07	−O−P−O− (1,3-PO_4, syn−syn)	eq−eq	−43.0 (exp)	this work
				−36.6 (DFT)	
	5.54	−O−V−O−P−O−	eq−ax	−0.20 (DFT)	
(II) $[\{Cu(phen)\}_2(VO_2(H_2O)_2)(H_2PO4)_2(PO_4)]_n$ (**2**)	3.46	−O−P−O− (1,3-PO_4, syn−syn)	eq−eq	−1.44 (exp)	
				−1.1 (DFT)	
	6.59	−O−V−O− (1,3-VO_4,syn−anti)	ax−ax	−0.01 DFT)	
(III) $[Cu_2(bipy)_2V_4O_{11}(PO_4)_2]$ 5 H_2O	3.19	−O− (1,1-PO_4); −O−P−O− (1,3-PO_4, syn−syn); −O−(1,1-VO_4)	eq−ax; eq−eq; eq−ax	+3.29 (DFT)	17
	4.10	−O−P−O−(1,3-PO_4, syn−anti); −O−P−O−(1,3-PO_4, syn−anti)	eq−eq; eq−ax	−0.63 (DFT)	
	5.38	−O−P−O− (1,3-PO_4, syn−anti); −O−P−O− (1,3-PO_4, syn−anti)	eq−ax; eq−ax	−2.23 (DFT)	
	5.01	−O−P−O− (1,3-PO_4, syn−anti); −O−P−O− (1,3-PO_4, syn−anti)	eq−eq; eq−eq	−46.14 (DFT)	
(IV) $[Cu_6(phen)_6(VO_2)_6(PO_4)_6(VO_2HO)_3]$	3.26	−O− (1,1-PO_4); −O− (1,1-PO_4)	eq−ax; ax−eq	−3.5 (exp)	21
(V) $[Cu(HINT)(VO_2)(PO_4)]$	3.15	−O− (1,1-PO_4); −O− (1,1-VO_5)−O−C−O− (HINT, syn−syn)	eq−eq; ax−ax; eq−eq	+36.0 (exp)	15
(VI) $[Cu_2(phen)_2(H_2O)_2(H_2PO4)_2](NO_3)_2$ 2 (H_2O)	5.01	−O−P−O− (1,3-PO_4, syn−anti); −O−P−O− (1,3-PO_4, syn−anti)	eq−eq; eq−eq	−8.0 (exp)	13
(VII) $[Cu_2(bipy)_2(V_4O_9)(PO4)_2(HPO_4)(H_2P_2O_7)]_n$ n(H_2O)	4.48	−O−P−O− (1,3-PO_4, syn−syn); −O−P−O− (1,3-PO_4, syn−syn); −O−V−O− (1,3-VO_4, syn−syn)	eq−eq; eq−eq; ax−ax	−28.8 (exp)	
(VIII) $[Cu_2(bipy)_2(VO_2)_2(PO4)_2]_n$	5.10	−O−P−O− (1,3-PO_4, anti−anti); −O−P−O− (1,3-PO_4, anti−anti)	eq−eq; eq−eq	−29.0 (exp)	
(IX) $[Cu_2(bipy)_2(\mu,\eta^2\text{-}HPO_4)(\mu,\eta^1\text{-}H_2PO_4)(\mu,\eta^2\text{-}H_2PO_4)]_n$	5.28	−O−P−O− (1,3-PO_4, syn−anti)	ax−eq	+0.14 (exp)	63
	3.32	−O−P−O− (1,3-PO_4, syn−syn); −O− (1,1-PO_4)	eq−eq; eq−ax	−5.3 (exp)	
(X) $[Cu_4(phen)_4(\mu_3,\eta^2\text{-}HPO_4)_2(\mu,\eta^2\text{-}H_2PO_4)_2(H_2PO_4)_2](H_2O)_4$	3.16	−O− (1,1-PO_4); −O− (1,1-PO_4)	eq−ax; eq−ax	+0.12 (exp)	
	5.06	−O−P−O− (1,3-PO_4, syn−syn); −O−P−O− (1,3-PO_4, anti−anti)	eq−eq; eq−eq	−1.32 (exp)	
	4.78	−O−P−O− (1,3-PO_4, syn−anti)	eq−ax	+ 0.1 (exp)	
(XI) $[Cu(phen)(\mu,\eta^2\text{-}HPO_4)(H_2O)_2]_n$	7.02	−O−P−O− (1,3-PO_4, anti−anti)	ax−ax	−5.86 (exp)	62

[a]Obtained from magnetic susceptibilities data and DFT calculations. d_{Cu-Cu} distances and J are given in Å and cm^{-1}, respectively. [b]exp: J value obtained from the fit of the experimental data; DFT: J value calculated using density functional theory.

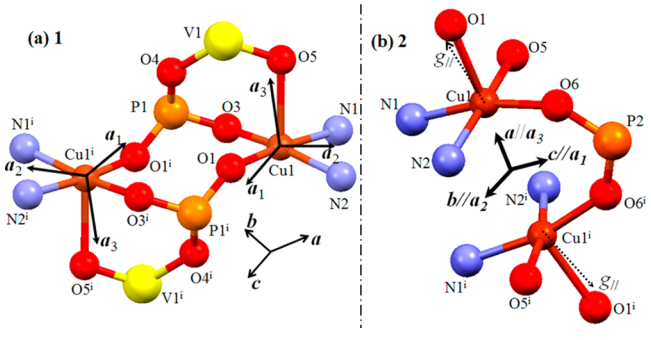

Figure 7. Molecular structure and principal directions of the **g**-tensors for the Cu sites in (a) **1** and (b) **2** obtained at Q-band. At the center of (b) a_1, a_2, and a_3 are the eigenvectors corresponding to the eigenvalues g_1, g_2, and g_3 of the crystalline **g**-matrix in Table 4, coincident with the ***abc*** crystalline axes. The directions a_1 and a_2 of **2** are not along the Cu−X bonds in the equatorial planes; angles CuN2−a_1 = 111.4°, and CuN2−a_2 = 25.2°.

Scheme 1. Exchange Pathways in the Four-Center Model for 1[a]

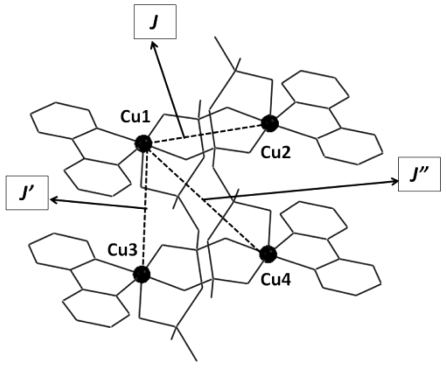

[a]Cu2 is Cu1[i] as the crystallographic position, and Cu3 is Cu1 as the crystallographic position.

[{Cu(phen)}$_2$(VO$_2$(H$_2$O)$_2$)(H$_2$PO4)$_2$ (PO$_4$)]$_n$ (**2**). The distances between neighboring copper atoms in **2** (Figure 2, Scheme 2)

DOI: 10.1021/ic503045d
Inorg. Chem. 2015, 54, 3805−3814

Scheme 2. Exchange Pathways in the Four-Center Model for 2

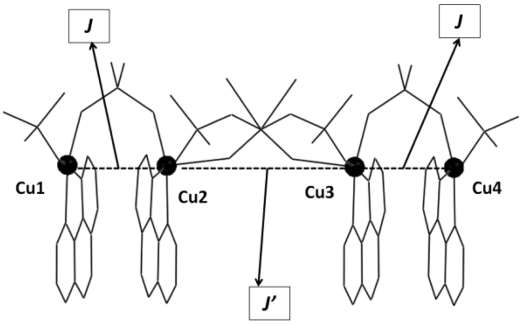

are 3.46 and 6.59 Å. However, while the structure of **1** displays dinuclear copper units perpendicular to the expansion of the chain, the structure of **2** displays the dinuclear moieties arranged along the chain expansion, with alternating double and single bridges. The shortest distance (3.46 Å), mediated by the single 1,3-PO_4 bridge, should mediate the stronger exchange interaction. For the second distance (6.59 Å) a VO_2 bridge exchange pathway involving several sigma bonds must be considered (Figure 2, Scheme 2).

If this second superexchange pathway is taken into account together with the first one, in principle an alternating chain model could be used as a model to fit the susceptibility data, with coupling constants J and J' for the exchange within and between dinuclear units.[55] However, fits using the calculations of Duffy and Barr[55] for alternate chains, together with the approximate expressions given by Hall et al.[56] and Hatfield,[57] gave inaccurate results. Since the model of Duffy requires the following condition $kT_{max}/|J| > \alpha$, and a T_{max} was not observed, a good fit could not be expected. Thus, the magnetic data of **2** were fitted with a simple Curie–Weiss equation:[43]

$$\chi(T) = \frac{C}{(T - \Theta)} \tag{6}$$

A good fit of $\chi^{-1}(T)$ to the data gives $C = Ng^2\mu_B{}^2S(S + 1)/3k_B = 4.3 \pm 0.1$ emu mol^{-1} K for the Curie constant and $\Theta = zJS(S + 1)/3k_B = -1.04 \pm 0.01$ K for the Curie–Weiss temperature, with $R = \sum[(\chi_M{}^{-1})_{exp} - (\chi_M{}^{-1})_{calc}]^2/\sum[(\chi_M{}^{-1})_{exp}]^2 = 2 \times 10^{-5}$. Figure 4a,b, containing the χT versus T data, χ^{-1} versus T data, and fits with eq 6, are typical of an AF system. Considering $S = 1/2$, $z = 2$, and $g = 2.2 \pm 0.1$, we obtained $J = -1.44 \pm 0.01$ cm^{-1}. This small value, together with the lack of a maximum in the $\chi(T)$ curve above 2 K, are indicative of the extremely weak AF interactions in **2**.

The equatorial–axial –O–V–O–P–O– exchange pathways in **1** and **2** and the axial–axial –O–V–O– pathway in **2** are less efficient for the exchange phenomena. Additionally, if the lengths of the diamagnetic paths are considered, a decrease of the magnetic exchange should be expected. The phosphate (–O–P–O–) bridges are the most efficient to support AF exchange couplings in both compounds, and the difference between the fitted exchange coupling parameters could be explained by the local coordination and the paths connecting the Cu ions in each compound. In **1** the d(x^2–y^2) orbitals of the Cu and Cu^i ions are in the same plane, and the Cu–P–Cu angle is 108.1° (Figure 1). These contribute to a more effective mixing of the d-orbitals of the copper ions through two –O–P–O– bridges. In contrast, in **2** the d(x^2–y^2) orbitals of each copper atom lie in parallel planes, with a Cu–P–Cu angle of 65.2°. These facts together with the presence of only one –O–P–O– bridge decreases the magnitude of the exchange phenomenon (Figure 2).

Electron Paramagnetic Resonance Results. The absence of a splitting of the EPR peaks indicates that the exchange interactions between dinuclear units are large enough to collapse the structures, due to the dinuclear (**D**) fine structure term.[45,49,58] The exchange interactions also collapse the hyperfine interactions with the nuclei of the copper ions ($I = 3/2$), the nitrogen ligands ($I = 1$), and also the resonance lines corresponding to the rotated copper ions in the case of compound **2**, giving rise to the single peak of the spectra.

Assuming an isotropic g-factor, the dipole–dipole (D_{dip} in the point dipole approximation) and the anisotropic exchange (D_{exch}) contributing to D are[44,59–61]

$$|D_{dip}| \approx \frac{3g^2\mu_B{}^2}{2R_{Cu-Cu}{}^3} \tag{7}$$

$$|D_{exch}| \approx \left(\frac{\Delta g}{g}\right)^2 |J| \tag{8}$$

More accurate expressions for D_{dip} and D_{exch} would not be of much help for our purpose,[44] and according to structural and magnetic results, $|D_{dip}|$ and $|D_{exch}|$ are 0.023 and 0.27 cm^{-1} for **1** and ~0.073 and 0.027 cm^{-1} for **2**. In the case of compound **1**, the observed collapse of the EPR peaks and the values estimated for the dipolar and anisotropic exchange contributions to D, allow to estimate $|J'| \geq 0.3$ cm^{-1}, supported by the already discussed –O–V–O–P–O– interdinuclear bridges. This value is ~1% of the dinuclear interaction and therefore very difficult to detect from the magnetic susceptibility data. In the case of compound **2**, a smaller interaction $|J'|$ is needed to collapse the dinuclear structure. Thus, the EPR results help to estimate the magnitudes of the smaller exchange couplings.

Density Functional Theory Calculations. For compound **1** a fragment of the 1D structure, composed of four copper centers, was used as model (Scheme 1). This fragment contains four possible exchange pathways with Cu–Cu distances of Cu1–Cu2 5.067 Å, Cu1–Cu3 5.536 Å, Cu1–Cu4 6.778 Å, and Cu2–Cu3 8.167 Å (Scheme 1). The last distance was not considered in the calculations; therefore, only three J values were estimated. To isolate each pathway, simultaneous diamagnetic substitution of two Cu^{II} centers by two Zn^{II} ions was used. For example, to evaluate J, Cu3 and Cu4 were substituted by diamagnetic cations, leading to the calculation of the ferromagnetic and the broken-symmetry configurations.

For compound **2** only two different exchange pathways can be defined in the structure with Cu–Cu distances of Cu1–Cu2 and Cu3–Cu4 = 3.465 Å and Cu2–Cu3 = 6.591 Å (Scheme 2). In the second model, the used fragment considered four copper centers, and the diamagnetic substitution method was also employed. The results of DFT calculations were $J = -36.60$ cm^{-1}, $J' = 0.20$ cm^{-1}, and $J'' \approx 0$ cm^{-1} for **1** and $J = -1.10$ cm^{-1} and $J' = 0.01$ cm^{-1} for **2**, both J' values being lower than 10% of the main exchange coupling. The information about complexes **1** and **2** obtained from susceptibility measurements and DFT calculations are summarized in Table 5 and compared with some related complexes.[13,15,17,21,62,63] The high coordination plasticity observed for 1,3-phosphate (1,3-PO_4), together with the scarce magnetic studies in the literature involving these systems, does not permit to obtain clearer magnetostructural correlations. A common problem in the related literature is that

DOI: 10.1021/ic503045d
Inorg. Chem. 2015, 54, 3805–3814

one, two, and three bridges are found between the spin carriers. This fact would lead to complementary or counter-complementary effects,[64] in the corresponding superexchange phenomena. For example, exchange pathways with only one 1,3-PO_4 bridge, in a syn−anti coordination mode and bonding the copper(II) centers in an axial−equatorial mode, leads to a weak ferromagnetic exchange as is observed in compounds **IX** and **X** in Table 5. However, when two 1,3-PO_4 bridges in a syn−anti coordination mode, both bonding the Cu^{II} centers in an equatorial−equatorial fashion, give rise to an AF exchange interaction, as observed in compounds **III** and **VI** in Table 5. Moreover for the same compound **III** where two 1,3-PO_4 bridges, in which the syn−anti conformation is maintained but the bonding becomes equatorial−axial, the AF phenomena becomes weaker. Finally, when three bridges are present, the counter-complementary effect avoids clear magnetostructural correlations.

CONCLUSIONS

New procedures of solvothermal synthesis are successfully exploited to prepare suitable single crystals for EPR measurements of two 1D Cu^{II} oxovanadium phosphates **1** and **2**. The fit of the susceptibility data allow calculating, with the used analytical models, only the strongest interactions $J = -43.0 \pm 0.5$ cm^{-1} for **1** and $J = -1.44 \pm 0.01$ cm^{-1} for **2**. Smaller couplings collapse the dinuclear structure of the EPR spectra and lower limits $|J'| \geq 0.3$ cm^{-1} for **1** and $|J'| \geq 0.15$ cm^{-1} for **2** can be estimated. DFT calculations allowed to calculate two different J values for each compound ($J = -36.60$ cm^{-1} and $J' = 0.20$ cm^{-1} for **1**, and $J = -1.10$ cm^{-1} and $J' = 0.01$ cm^{-1} for **2**). For compound **2** the second interaction defined by J' is small, being in the range of the uncertainties of the calculations. Thus, DFT results are in good agreement with magnetic and EPR results, providing in addition the signs of the small exchange couplings J', which are not accessible from EPR.

ASSOCIATED CONTENT

Supporting Information

Illustration of $\pi-\pi$ intrachain interaction, illustration of $\pi-\pi$ stacking interactions, and crystallographic data of **1** and **2** in CIF format. This material is available free of charge via the Internet at http://pubs.acs.org. The Cambridge refcodes of compounds **1** and **2** are XIWSIF[24] and XACTAX,[25] respectively.

AUTHOR INFORMATION

Corresponding Authors

*E-mail: diego.venegas@usach.cl. (D.V.-Y.)
*E-mail: espodine@ciq.uchile.cl. (E.S.)
*E-mail: santana@ufg.br. (R.C.S.)

Notes

The authors declare no competing financial interest.

ACKNOWLEDGMENTS

Authors are grateful to Dr. O. R. Nascimento (Instituto de Física de São Carlos, USP, Brazil) for allowing the use of EPR facilities. This work was supported by Projects CAI+D-UNL in Argentina and CNPQ in Brazil. R.C. is a member of CONICET, Argentina. The research was also partially financed by FB0807 Project (CEDENNA) and by Projects FONDECYT 1120001 and 1120004. The authors also acknowledge support from the International Collaboration Program LIA-MIF CNRS 836. Powered@NLHPC. We received partial support from the Supercomputing Infrastructure of the National Laboratory for High Performance Computing, NLHPC (ECM-02), Center for Mathematical Modeling (CMM), Universidad de Chile.

REFERENCES

(1) Finn, R. C.; Zubieta, J. *J. Phys. Chem. Solids* **2001**, *62*, 1513−1523.
(2) Amorós, P.; Marcos, M. D.; Beltrán-Porter, A.; Beltrán-Porter, D. *Curr. Opin. Solid State Mater. Sci.* **1999**, *4*, 123−131.
(3) Finn, R.; Zubieta, J. *Chem. Commun.* **2000**, *2*, 1321−1322.
(4) Feng, S.; Xu, R. *Acc. Chem. Res.* **2001**, *34*, 239−247.
(5) Qin, C.; Xu, L.; Wei, Y.; Wang, X.; Li, F. *Inorg. Chem.* **2003**, *42*, 3107−3110.
(6) Yucesan, G.; Golub, V.; O'Connor, C. J.; Zubieta, J. *Solid State Sci.* **2005**, *7*, 133−139.
(7) Soghomonian, V.; Haushalter, R. C.; Zubieta, J.; O'Connor, C. J. *Inorg. Chem.* **1996**, *35*, 2826−2830.
(8) Bircsak, Z.; Harrison, W. T. A. *Inorg. Chem.* **1998**, *3208*, 3204−3208.
(9) Shi, F. N.; Almeida Paz, F. A.; Rocha, J.; Klinowski, J.; Trindade, T. *Inorg. Chim. Acta* **2005**, *358*, 927−932.
(10) Zhang, S. F.; Liu, G. Z.; Zheng, S. T.; Yang, G. Y. *J. Solid State Chem.* **2007**, *180*, 1943−1948.
(11) Lin, B.-Z.; Liu, S.-X. *J. Chem. Soc., Dalton Trans.* **2002**, 865−869.
(12) Zhang, X.-M.; Wu, H.-S.; Gao, S.; Chen, X.-M. *J. Solid State Chem.* **2003**, *176*, 69−75.
(13) Moreno, Y.; Vega, A.; Ushak, S.; Baggio, R.; Peña, O.; Le Fur, E.; Pivan, J.-Y.; Spodine, E. *J. Mater. Chem.* **2003**, *13*, 2381.
(14) Koo, B.-K.; Ouellette, W.; Burkholder, E. M.; Golub, V.; O'Connor, C. J.; Zubieta, J. *Solid State Sci.* **2004**, *6*, 461−468.
(15) Wang, C.-M.; Chuang, Y.-L.; Chuang, S.-T.; Lii, K.-H. *J. Solid State Chem.* **2004**, *177*, 2305−2310.
(16) Spodine, E.; Venegas-Yazigi, D.; Ushak, S.; Le Fur, E.; Pivan, J. Y. *Phys. B* **2006**, *384*, 120−122.
(17) Spodine, E.; Venegas-Yazigi, D.; Ushak, S.; Paredes-García, V.; Saldias, M.; Le Fur, E.; Pivan, J. Y. *Polyhedron* **2007**, *26*, 2121−2125.
(18) Ushak, S.; Spodine, E.; Venegas-Yazigi, D.; Le Fur, E.; Pivan, J. Y. *Microporous Mesoporous Mater.* **2006**, *94*, 50−55.
(19) Ushak, S.; Spodine, E.; Le Fur, E.; Venegas-Yazigi, D.; Pivan, J.-Y.; Schnelle, W.; Cardoso-Gil, R.; Kniep, R. *Inorg. Chem.* **2006**, *45*, 5393−5398.
(20) Saldias, M.; Paredes-Garcia, V.; Vega, A.; Cañon-Mancisidor, W.; Le Fur, E.; Venegas-Yazigi, D.; Spodine, E. *Polyhedron* **2012**, *41*, 120−126.
(21) Silva-Galaz, C.; Saldias, M.; Freire, E.; Baggio, R.; Le Fur, E.; Paredes-Garcia, V.; Spodine, E.; Venegas-Yazigi, D. *J. Mol. Struct.* **2013**, *1051*, 205−210.
(22) Marino, N.; Ikotun, O. F.; Julve, M.; Lloret, F.; Cano, J.; Doyle, R. P. *Inorg. Chem.* **2011**, *50*, 378−389.
(23) Tripuramallu, B. K.; Mukherjee, S.; Das, S. K. *Cryst. Growth Des.* **2012**, *12*, 5579−5597.
(24) Shi, Z.; Feng, S.; Zhang, L.; Yang, G.; Hua, J. *Chem. Mater.* **2000**, *12*, 2930−2935.
(25) Cui, Y.; Li, G.; Meng, H.; Xing, Y.; Ding, H.; Sun, J.; Liu, L.; Pang, W. *Inorg. Chem. Commun.* **2004**, *7*, 909−911.
(26) Ushak, S.; Spodine, E.; Venegas-Yazigi, D.; Fur, E.; Le Pivan, J. Y.; Peña, O.; Cardoso-Gil, R.; Kniep, R. *J. Mater. Chem.* **2005**, *15*, 4529.
(27) *SAINTPLUS,* Version 6.02; Brucker AXS: Madison, WI, 1999.
(28) *SHELXTL,* Version 5.1; Brucker AXS: Madison, WI, 1998.
(29) Sheldrick, G. M. *SHELXL-97,* Program for Crystal Structure Refinement; University of Göttingen: Germany, 1997.
(30) Earnshaw, A. *Introduction to Magnetochemistry;* Academic Press: England, 1968.
(31) Giacovazzo, C. *Fundamentals of Crystallography;* Giacovazzo, C., Ed.; Oxford University Press: Oxford, U.K., 1992; pp 68−69.
(32) Suh, I. H.; Park, Y. S.; Kim, J. G. *J. Appl. Crystallogr.* **2000**, *33*, 994−994.

DOI: 10.1021/ic503045d
Inorg. Chem. 2015, 54, 3805−3814

(33) Stoll, S.; Schweiger, A. *J. Magn. Reson.* **2006**, *178*, 42−55.
(34) *Matlab;* The Mathworks Inc.: Natick, MA. http://www.mathworks.com/products/matlab/.
(35) Becke, A. *J. Chem. Phys.* **1993**, *98*, 5648−5652.
(36) Schafer, A.; Huber, C.; Ahlrichs, R. *J. Chem. Phys.* **1994**, *100*, 5829−5835.
(37) *Jaguar,* Version 5.5; Schrödinger, LLC: Portland, OR, 2005.
(38) *Gaussian 09;* Gaussian Inc.: Pittsburgh, PA, 2009.
(39) Ruiz, E.; Alvarez, S.; Cano, J.; Polo, V. *J. Chem. Phys.* **2005**, *123*, 164110.
(40) Ruiz, E. *Struct. Bonding (Berlin, Ger.)* **2004**, *113*, 71−102.
(41) Brown, I. D.; Altermatt, D. *Acta Crystallogr., Sect. B: Struct. Sci.* **1985**, *41*, 244−247.
(42) Addison, A. W.; Rao, T. N.; Reedijk, J.; van Rijn, J.; Verschoor, G. C. *J. Chem. Soc., Dalton Trans.* **1984**, 1349−1356.
(43) Kahn, O. *Molecular Magnetism;* Wiley-VCH Inc.: Weinheim, Germany, 1993.
(44) Bencini, A.; Gatteschi, D. *Electron Paramagnetic Resonance of Exchange Coupled Systems;* Springer-Verlag: Berlin, Germany, 1990.
(45) Calvo, R. *Appl. Magn. Reson.* **2007**, *31*, 271−299.
(46) Napolitano, L. M. B.; Nascimento, O.; Cabaleiro, S.; Castro, J.; Calvo, R. *Phys. Rev. B* **2008**, *77*, 214423.
(47) Perec, M.; Baggio, R.; Sartoris, R. P.; Santana, R. C.; Peña, O.; Calvo, R. *Inorg. Chem.* **2010**, *49*, 695−703.
(48) Calvo, R.; Abud, J. E.; Sartoris, R. P.; Santana, R. C. *Phys. Rev. B* **2011**, *84*, 104433.
(49) Sartoris, R. P.; Nascimento, O. R.; Santana, R. C.; Perec, M.; Baggio, R. F.; Calvo, R. *Dalton Trans.* **2015**, *44*, 4732−4743.
(50) Calvo, R.; Mesa, M. *Phys. Rev. B* **1983**, *28*, 1244−1248.
(51) Calvo, R.; Mesa, M. A.; Oliva, G.; Zukerman-Schpector, J.; Nascimento, O. R.; Tovar, M.; Arce, R. *J. Chem. Phys.* **1984**, *81*, 4584−4591.
(52) Zeiger, H. J.; Pratt, G. W. *Magnetic Interactions in Solids;* Clarendon: Oxford, U.K., 1973; p 103.
(53) Passeggi, M. C. G.; Calvo, R. *J. Magn. Reson.* **1995**, *114*, 1−11.
(54) Bleaney, B.; Bowers, K. D. *Proc. R. Soc. London, Ser. A* **1952**, *214*, 451−465.
(55) Duffy, W.; Barr, K. P. *Phys. Rev. B* **1968**, *165*, 647−654.
(56) Hall, J. W.; Marsh, W. E.; Weller, R. R.; Hatfield, W. E. *Inorg. Chem.* **1981**, *20*, 1033−1037.
(57) Hatfield, W. E. *J. Appl. Phys.* **1981**, *52*, 1985−1990.
(58) Anderson, P. W.; Weiss, P. R. *Rev. Mod. Phys.* **1953**, *25*, 269−276.
(59) Abragam, A.; Bleaney, B. *Electron Paramagnetic Resonance of Transition Ions;* Oxford University Press: Cambridge, U.K., 1970.
(60) Ozarowski, A. *Inorg. Chem.* **2008**, *47*, 9760−9762.
(61) Moriya, T. *Phys. Rev.* **1960**, *120*, 91−98.
(62) Youngme, S.; Phuengphai, P.; Pakawatchai, C.; Van Albada, G. A.; Tanase, S.; Mutikainen, I.; Turpeinen, U.; Reedijk, J. *Inorg. Chem. Commun.* **2005**, *8*, 335−338.
(63) Phuengphai, P.; Youngme, S.; Chaichit, N.; Pakawatchai, C.; van Albada, G. A.; Quesada, M.; Reedijk, J. *Polyhedron* **2006**, *25*, 2198−2206.
(64) Sarkar, S.; Majumder, S.; Sasmal, S.; Carrella, L.; Rentschler, E.; Mohanta, S. *Polyhedron* **2013**, *50*, 270−282 and references there in..

DOI: 10.1021/ic503045d
Inorg. Chem. 2015, 54, 3805−3814